Journal of Solid State Chemistry **160,** 100–107 (2001)
doi:10.1006/jssc.2001.9199, available online at http://www.idealibrary.com on IDEAL®

Characterization of the Thermal Behavior of Li–Fe–Tartrate Gels (Molar Ratio Li/Fe $\leq$ 1/5)

J. M. Yang, W. J. Tsuo, and F. S. Yen

Department of Mineral and Petroleum Engineering, National Cheng Kung University, Tainan, Taiwan 70101, Republic of china

Received December 3, 2000; in revised form March 22, 2001; accepted April 9, 2001; published online July 3, 2001

The differential thermal analysis/thermogravimetric analysis characteristics of Li–Fe xerogels prepared by the tartrate gel technique are examined. Monophase lithium ferrospinel powders can be obtained by adjusting the calcining temperatures at 200–300°C and 550°C for the xerogel, if α-Fe_2O_3 was absent during the processing. The former temperature range resulted from the thermal reaction of γ-Fe_2O_3 with lithium. The latter was attributed to the thermal reaction of Li-containing γ-Fe_2O_3 (Li–γ-Fe_2O_3) with lithium. An increase in the amount of the former formed can substantially decrease that for the latter. The thermal reaction for forming lithium ferrite can be topotactic. More importantly, it may be triggered by the phase transformation.

1. INTRODUCTION

Lithium ferrospinel (LFS), known as lithium ferrite, $Li_{0.5}Fe_{2.5}O_4$, crystal structure 1–3 inverse spinel, FCC with symmetry group F$d3m$ (O_h^7), is one of the well-known ferrites. It is essentially a magnetite that contains a certain amount of lithium in substitution for $\frac{1}{4}$ iron in its octahedral ($B-$) site (1). The tetrahedral (A) sublattices are fully occupied by Fe^{3+} ions, and the octahedral (B) sublattices are occupied by Li^+ and Fe^{3+} ions in 1:3 proportion, $(Fe)_A[Li_{0.5}Fe_{1.5}]_BO_4$ (2). Having a relatively low microwave dielectric loss (3) and showing a squarish hysteresis loop as well as having a high saturation magnetization, 2.6 μ_B/formula unit, and a superior temperature performance due to its higher Curie temperature ($T_c = 680$°C) (3–5), lithium ferrite has become a very promising material for making microwave devices, especially as a replacement for YIG garnets owing to their low cost of fabrication.

The solid-state thermal reaction, using α-Fe_2O_3 and Li_2CO_3 or a compound of Li^+ as the starting materials, has been employed as the main process in manufacturing ferrite powders (6). Since the diffusion processes between the ingredients are the main formation mechanism encountered in the processing, details such as mixing homogeneity and thermal reaction conditions are crucial. During the thermal reaction $LiFeO_2$ will be formed. Or,

$$Li_2CO_{3(s)} + \alpha\text{-}Fe_2O_{3(s)} \rightarrow 2LiFeO_{2(s)} + CO_{2(g)} \quad [1]$$

$$LiFeO_{2(s)} + 2\alpha\text{-}Fe_2O_{3(s)} \rightarrow LiFe_5O_{8(s)}. \quad [2]$$

To accomplish reaction [2], annealing for a long time at a temperature above 800°C is necessary. Powders thus obtained are of coarser size. The densification of the ceramics using the powder must involve an even higher sintering temperature (> 1100°C). It is obvious that it causes a loss in lithium fraction as well as the formation of α-Fe_2O_3 and a defect structure of the ferrite. Subsequently the ceramics thus formed are lower in magnetization (5–7).

A number of nonconventional processes have been considered to substitute the conventional solid-state reaction method to produce fine-size lithium ferrite powders at lower temperatures. These processes include obtaining precursors by chemical coprecipitation (8) and organometallic compounds (9), growing ferrite by hydrothermal systems (10), techniques of glass ceramics (11), freeze drying (12), and spray drying (13, 14), and some improved solid-state reaction methods (15, 16). These processes attempt to yield finer-sized powders by a more intimate mixing of the starting materials.

Similar to LFS, the structure of γ-Fe_2O_3 can also be described as an inverse spinel structure. But vacancies in its octahedral sites are noted, giving a $\triangle$-3-type ($\triangle_{1/3}\ Fe_{8/3}^{3+}O_4$) structure (17). It is assumed that if Li^+ ions can diffuse into γ-Fe_2O_3 structure directly during the process of LFS synthesis, a topotactic reaction (TTR) (18) can be conducted due to the structural similarity between the reactants and products. An energy-saving process of producing fine-size powders can be achieved at lower temperatures.

The mineral synthesis using TTR techniques has been reported previously. For examples, in the synthesis of α-$NaFeO_2$, the structural similarities of γ-Fe_2O_3 with α-$NaFeO_2$ and α-Fe_2O_3 with β-$NaFeO_2$ were noted. Consequently α-$NaFeO_2$ was obtained directly using γ-Fe_2O_3 and Na_2CO_3 as starting materials, or via formation of

0022-4596/01 $35.00

β-$NaFeO_2$ in advance using α-Fe_2O_3 and Na_2CO_3 as starting materials and then α-$NaFeO_2$ is obtained through the phase transformation of β- to α-$NaFeO_2$ (19).

Sano and Tamaura (15) prepared (Li,Mn) ferrites at 650°C using ultrafine γ-Fe_2O_3 powders (10 nm in mean diameter) and $LiMnO_4$ as the starting materials. The thermal reaction can be divided into two steps. (1) Topotactic reaction at 390–560°C: the manganese ions diffuse into the lattice of γ-Fe_2O_3 to form (Li,Mn) ferrites. (2) Traditional solid-state reaction at 560–650°C: the residual $LiMnO_4$ particles reacted with α-Fe_2O_3 (transformed from γ-Fe_2O_3) to form (Li,Mn) ferrites. Similar results were obtained by Rane *et al.* (20) in preparation of Mg ferrites using ultrafine γ-Fe_2O_3 powders (10–30 nm) and commercial α-Fe_2O_3 powders (1–2 μm) for comparison. For the former, mono phase ferrites with high magnetization were obtained at ~ 1000°C, while for the latter, a higher reaction temperature was needed.

The nonconventional processes aim at lowering the thermal reaction temperature by developing techniques of mixing the starting materials at atomic scale by which not only the reaction rate is increased but also the homogeneity in product phases is improved. The tartrate gel technique by which the organometallic compounds can be prepared has been employed as one of the nonconventional processes in preparing ferrite powders (15, 21, 22). These studies have shown that formation of LFS by the techniques can be achieved through the TTR mechanism. Lithium ions diffuse into the structure of γ-Fe_2O_3 at temperatures below 600°C (22). Very similar to the process of (Li,Mn) ferrite formation (15), the thermal reaction can be divided into TTR at lower temperatures and the solid-state reaction at higher temperatures. However, neither are studies dealing with the relationships between the two steps defined nor is the role of lithium in the two steps clear.

γ-Fe_2O_3 is thermodynamically a metastable mineral at room temperature of inverse spinel structure with vacancies distributed in its *B*-sites. The ratio of the vacancy ($\triangle$) to the Fe^{3+} in the *B*-site is 1:5. When the mineral is formed at lower temperature, the ordering of vacancy causes a decrease in the free energy and it is presumably stabilized (16). However, a phase transformation takes place when the temperature rises and the γ phase transforms to the stable α-Fe_2O_3 phase. Studies indicate that the transformation occurs in the temperature range from 350 to 600°C whereas in the case of the γ phase obtained by decomposition of salts, the transformation initiates at temperatures ranging from 400 to 450°C (21–23). Studies have also revealed that once the cations are present in the structure, the phase transformation temperature would increase. For examples, with 0.2 mol% Na present the temperature can increase to > 600°C (24). Similar studies were reported for the presence of ≤ 1 mol% of Co, Ni, Zn, Cu, and Mn (540–650°C) (26), and 0.1 mol% of La, Pr, and Nd (~ 615°C) (27). Further, it can be stabilized if Ba^{2+} ions enter the structure (28). The phase transition is generally manifested by a discontinuous variation in some property where a change in temperature occurs. Recently, the dimension (size) of a finite-size system has also been recognized as a "parameter" responsible for certain types of phase transitions (29–32). It is interesting to note that the $\gamma \rightarrow \alpha$-$Fe_2O_3$ transition can be induced by size (33). Above 30 nm, the stable phase was α-Fe_2O_3 (rhombohedral, corundum structure), whereas below 30 nm it was found to be γ-Fe_2O_3 (cubic, spinel structure) (34).

Investigation (27) of the presence of Li in the γ-Fe_2O_3 structure has revealed that it can be a solid solution of γ-Fe_2O_3 (33%) and $LiFe_5O_8$ (67%). It is tetragonal and a superstructure equivalent to that found in crystalline γ-Fe_2O_3 with $c = 3a$. The solid solution decomposes at 850°C (27) into the two phases.

An attempt is made to investigate the thermal behavior and the relationships between the presence of γ-Fe_2O_3 and lithium-containing γ-Fe_2O_3 (hereafter designated as Li–γ-Fe_2O_3) during the formation of LFS using tartrate techniques. Studies are focused on how the α-Fe_2O_3 phase can be eliminated on the basis of the formation mechanism in which LFS is formed via TTR of the two spinel–γ-Fe_2O_3's. In order to promote the thermal reaction and to allow an easy observation for the phenomena, pretreatments at lower temperatures, 200 and 300°C, for 2 hrs are done so that the organic volatile portions can be removed in advance. Further, as the reaction system is simplified, it is anticipated that the TTR for forming LFS may proceed more smoothly.

2. EXPERIMENTAL PROCEDURE

2.1. Precursor Preparation

Tartrate techniques (15, 22, 23) were employed to synthesize LFS. Two solutions were prepared to fulfill the process. (1) A solution containing Li^+ and Fe^{3+} with concentrations 0.08 and 0.2 mol/L, respectively: Lithium acetate dihydrate ($CH_3COOLi \cdot 2H_2O$, Fluka, $> 99\%$) and ferric nitrate nonahydrate ($Fe(NO_3)_3 \cdot 9H_2O$, Merck, $> 99\%$) were dissolved in and then adjusted with ethyl alcohol (Seoul, 99.5%) to form the solution (molar ratio of $Li^+ : Fe^{3+} = 1:5$). (2) Tartaric acid solution: L-(+)-Tartaric acid ($C_4H_6O_6$), Fluka, $> 99.5\%$) was dissolved in ethyl alcohol to make a solution with 0.832 mol/L tartaric acid. Tartrate precipitates were then obtained by titrating one volume unit of solution 1 into one volume unit of stirred tartaric acid solution 2. It should be noted that the tartaric acid used for titration was 30% in excess over the stoichiometric amount needed to meet the charge balance. The precipitates remained in the solution (in the original container) for 1 hr with constant stirring to ensure that the reaction was complete. It was then vacuum oven dried for

24 hrs. The dried gel was ground to -200 mesh (< 74 μm) and used as the starting material for the study.

Additional gel powders of pure Li tartrate were obtained separately following identical procedures.

2.2. Calcined Powders

A preliminary test using differential thermal analysis/thermogravimetric analysis (DTA/TG) compared with phase analysis using X-ray diffraction (XRD) was made to evaluate the necessary temperature and the process for calcination of the gel powder. Additionally, pretreatments of the gel powder at 200 and 300°C for 2 hrs were done to remove the organic volatiles and made the examination easy.

2.3. Powder Characterization

Thermal behavior examinations of both the xerogel powder and the heat pretreated powder were conducted using DTA/TG techniques (Setaram TGA92) in air at a heating rate of 5°C/min. The reference sample was well crystallized α-Al_2O_3 powder. The crystalline phase identification for the calcined powders was performed by XRD powder methods using Ni-filtered Cu$K\alpha$ radiation, 30 kV × 20 mA (Rigaku, Tokyo).

3. RESULTS AND DISCUSSION

3.1. Thermal Behavior of Individual Lithium and Iron Precipitates

The thermal behavior of Fe gels prepared by tartrate gel techniques has been reported previously (23). Two main phases, γ- and α-Fe_2O_3, were found to occur in the temperature ranges of 250–275°C and 440–460°C, respectively. Meanwhile during the γ phase formation, a manifest weight-gain reaction occurs, implying a simultaneous oxidation reaction, $Fe^{2+} \rightarrow Fe^{3+}$, along with the removal of organic volatile. Similar results were observed in this study. Since the $Fe^{2+} \rightarrow Fe^{3+}$ reaction can be induced by the oxidation of magnetite (Fe_3O_4) and the phase identification revealed that there is no significant difference in XRD characteristics between the oxidized phase and the γ-Fe_2O_3 for the samples calcined at 200 to 250°C, it is suspected that the precursor can be magnetite. Further, a preliminary examination of color variation of the calcined sample also showed that the color was brownish black instead of brown and the weight gain can be attributed to the oxidation of magnetite (Fe_3O_4) to form γ-Fe_2O_3.

Figure 1 shows DTA/TG curves of pure Li^+-containing gel powders. Three exothermic reactions occurred at temperatures 270–325 (Ix), 325–380 (IIIx), and 425 ~ 475°C (IVx), indicating that at least three reactions occurred. The exothermic reaction Ix resulted from the thermal decomposition of the tartrate. During the decomposition, an endothermic reaction took place at 270–325°C (IIn) that intercepted the high-temperature ends of peak Ix. The endothermic IIn was accompanied by a weight gain (IIg). The corresponding XRD phase identification reflecting the DTA/TG behavior of the sample using samples calcined at the scheduled temperature (for 1 hr) revealed that (Fig. 2)

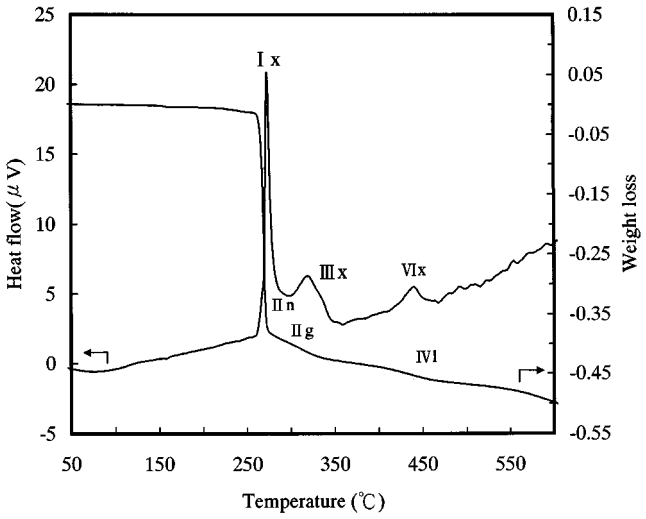

FIG. 1. DTA/TG profiles of Li precipitate with a heating rate of 5°C min^{-1} in air atmosphere.

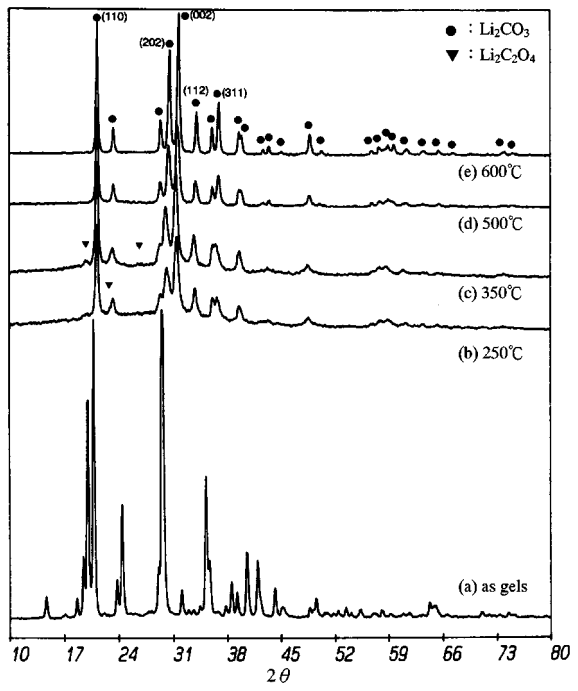

FIG. 2. XRD patterns of Li precipitate (a) as received and calcined at (b) 250°C, (c) 350°C, (d) 500°C, and (e) 600°C for 1 h with a heating rate of 5°C min^{-1}.

a step of amorphous state occurred with the Li gel after the as-purchased gels were thermally treated. At $\sim 250^{\circ}C$ or lower, then the formation of lithium carbonate (Li_2CO_3) occurred (Fig. 1, IIg, and Fig. 2b), and it coexisted with the amorphous phase until the appearance of lithium acetate (LiC_2O_4) at 350°C (Fig. 1, IIIx, and Figs. 2b and 2c). As the temperature increased, the acetate decomposed to form lithium carbonate, IVx, accompanied with a weight loss, IVl. After that the carbonate became the only phase (Fig. 1, IVx and IVl, Fig. 2d).

3.2. *Thermal Behaviors of Li–Fe Coprecipitates*

Figure 3 shows DTA/TG curves of the Li–Fe coprecipitates at a 5°C/min heating rate. The exotherm IIx presumably included the thermal reactions that occurred in the exothem Ix in Fig. 1 and resulted a wider peak. When compared with the corresponding XRD patterns of the calcined powders (Fig. 4), it is found that the tartrate gel is amorphous. The γ-Fe_2O_3 transformation from the tartrate gel may occur at temperatures lower than 300°C which is possibly comparable to IIIn–IVx on the DTA profile (Fig. 3). This is because a weight gain (IVg) and, after that, the TG approaching stable are observed. Meanwhile, the formation of lithium carbonate was also observed (Fig. 4b). However, compared to Fig. 2, it is obvious that the quantity of Li_2CO_3 formation was substantially smaller, indicating that a large amount of Li^+ prevailed as ions or entered into the structure of γ-Fe_2O_3. At exothermic Vx the Li–Fe spinels were formed. The spinels may consist of stoichiometric lithium ferrite (LFS), α-$LiFe_5O_8$, and Li-containing γ-Fe_2O_3's (designated as Li–γ-Fe_2O_3). α-Fe_2O_3, which can transform from α-Fe_2O_3 (24), appeared in the sample calcined at 350°C/2 hrs, corresponding to the exothermic reaction VIx (360–450°C). It is found that α-Fe_2O_3 thus formed persisted despite the increase in temperature. Further, it became more evident after calcination at 600°C/2 hrs for the sample. Obviously, the increase in α-Fe_2O_3 formation at a later stage resulted from the decomposition of Li–γ-Fe_2O_3 (24–27), implying that the exothermic reaction Vx (300–360°C) may reflect the initiation of formation of LFS (Li ferrospinel) as well as Li–γ-Fe_2O_3. It is noted that the Li–γ-Fe_2O_3 may become obscure, reacting with Li^+ to form LFS, if heat treatments are conducted at a temperature near 600°C (referred to Fig. 6). Consequently, the thermal behavior of the Li–Fe coprecipitates can be briefly concluded as shown in Table 1.

It should be noted that the exothermic peak Vx ($\sim 325^{\circ}C$) may reflect the topotactic reaction (TTR) between (spinel-) γ-Fe_2O_3 and Li^+ to form (spinel-) LFS and then the formation of α-Fe_2O_3 transformed from residual γ-Fe_2O_3 at VIx ($\sim 450^{\circ}C$) (Figs. 4d and 4e). The Li–γ-Fe_2O_3 at exotherm Vx (300–360°C) eventually reacts with

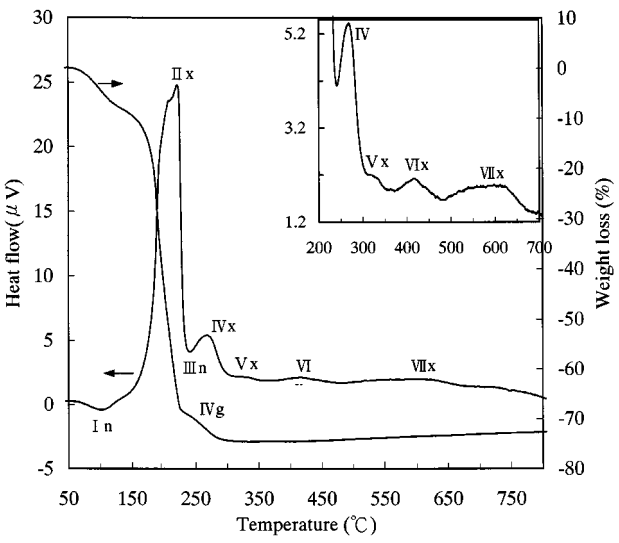

FIG. 3. DTA/TG profiles of the Li–Fe coprecipitate obtained by tartrate techniques. The heating rate is 5°C min^{-1} in air atmosphere.

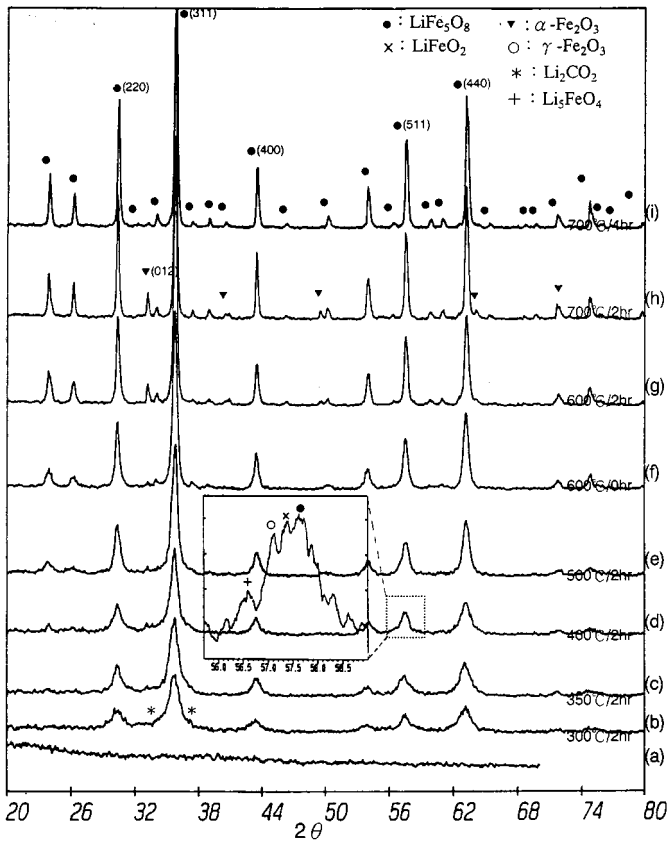

FIG. 4. XRD patterns of the calcined powders obtained by calcination of Li–Fe coprecipitates via tartrate techniques with a heating rate of 5°C min^{-1}. (a) as received, calcined at (b) 300°C, (c) 350°C, (d) 400°C, (e) 500°C, (g) 600°C, and (h) 700°C for 2 hrs, calcined at (f) 600°C for 0 hr, and calcined at (i) 700°C for 4 hrs.

TABLE 1
Thermal Reaction of Li–Fe Gel (Heating Rate, 5°C/min)

	Thermal reaction (°C)	Reaction[a]
IIIn	230	Li_2CO_3, Fe_3O_4(?)
IVx	250–300	$Fe_3O_4 \rightarrow \gamma$-$Fe_2O_3$
Vx	300–360	$Fe_3O_4 + Li^+ \rightarrow Li$-$\gamma$-$Fe_2O_3$
VIx	~ 400	$Li^+ + \gamma$-$Fe_2O_3 \rightarrow$ LFS
	~ 450	$\gamma \rightarrow \alpha$-$Fe_2O_3$
VIIx	480–600	Li-γ-$Fe_2O_3 + Li^+ \rightarrow$ LFS
	670(?)–680	Li-γ-$Fe_2O_3 \rightarrow$ LFS + α-Fe_2O_3

[a] LFS = $LiFe_5O_8$.

Li^+ to form (spinel-) LFS at temperatures ranging from about 480 to 600°C, before the second appearance of α-Fe_2O_3 (VIIx); if not, it would transform into LFS and α-Fe_2O_3 (35, 36) at > 600°C(?) (Figs 4f and 4g). However, whether the reaction is TTR (Expression [3]) or it is a two-step reaction (Expressions [4.1] and [4.2]) needs further study. However, the possibility of forming LFS via α-Fe_2O_3 plus Li^+ can be limited. This is why a higher temperature is required to perform the LFS formation process for the α-Fe_2O_3. Or, it is important to find that both α-Fe_2O_3 phases formed from transformation of γ-Fe_2O_3 and Li–γ-Fe_2O_3 can persist after calcination at temperatures > 700°C (Fig. 4i).

$$Li\text{-}\gamma\text{-}Fe_2O_{3(s)} + Li^+ \rightarrow LiFe_5O_{8(s)} \qquad [3]$$

$$Li\text{-}\gamma\text{-}Fe_2O_{3(s)} \rightarrow LiFe_5O_{8(s)} + \gamma\text{-}Fe_2O_{3(s)} \qquad [4.1]$$

$$\gamma\text{-}Fe_2O_{3(s)} + Li^+ \rightarrow LiFe_5O_{8(s)}. \qquad [4.2]$$

3.3. Heat Pretreatments at Lower Temperatures

Attempts were made to evaluate the possibility of eliminating α-Fe_2O_3 formation by heat treatments at lower temperatures ahead of that for the transformation of γ- and Li–γ- to α-Fe_2O_3. The experiment was based on the fact that LFS can be obtained at temperatures before the occurrence of phase transformation (37).

Figure 5 displays two sets of DTA/TG curves of the Li–Fe gels heat pretreated at 200°C but for different annealing times: 1 and 2 hrs (Fig. 5, exotherms Vx, VIx, and VIIx for the 2-hr sample, and Vx′, VIx′, and VIIx′ for the 1-hr sample). Since the samples were heat pretreated at 200°C, the exothermic reaction IIx that appeared in Fig. 3 had been mostly removed. The rest of the exotherms that occurred in Fig. 3 remained, except VIIx and VIIx′ which eventually diminished and disclosed identical physical meaning. Of the exotherms for the two samples, the first IVx and IVx′, (using identical notations as shown in Fig. 3) and the accompanying weight gain indicated the formation of γ-Fe_2O_3. LFS and Li–γ-Fe_2O_3 appeared in the second exotherm, Vx

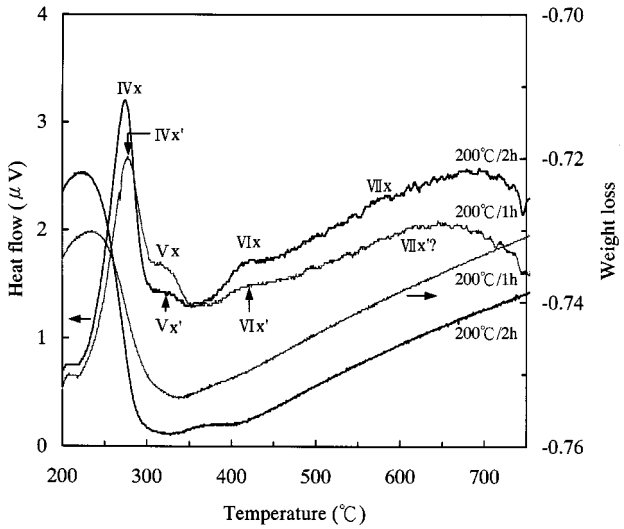

FIG. 5. DTA/TG profiles of the samples thermally pretreated at 200°C/1 hr and 200°C/2 hrs with a heating rate of 5°C min^{-1} in air atmosphere.

(and Vx′). Further LFS synthesis may occur at the first portion of the exotherm VIx (VIx′). After that the first appearance of α-Fe_2O_3 came about. Li–γ-Fe_2O_3 reacted with Li^+ to form LFS at the first portion of the exotherm VIIx (VIIx′). and it was followed sequentially by the second appearance of α-Fe_2O_3.

A detailed examination of the DTA/TG curves of the two samples shows a substantial discrepancy between the two curves. The exotherms IVx and VIx of the sample annealed for 2 hrs are higher than that of sample annealed for 1 hr, while Vx remained lower (Fig. 5). Apparently, a higher amount of γ-Fe_2O_3 formation actually results in a lower amount of Li–γ-Fe_2O_3 formation, and subsequently, the amount of α-Fe_2O_3 occurring at VIx will be higher and that at VIIx will be lower. This provided a possible process to eliminate the presence of α-Fe_2O_3 during the synthesis of LFS powders using tartrate techniques.

Figure 6 demonstrates the effect of heat pretreatment on the elimination of α-Fe_2O_3 formation during the LFS synthesis. The temperature and the duration selected for annealing processes were 200 and 300°C/2 hrs and 550°C/2 hrs for γ- and Li–γ-Fe_2O_3, respectively. To study the effect of eliminating α-Fe_2O_3 formation, the treated samples were annealed at 500 and 600°C for 2 hrs, because the residual γ- and Li–γ-Fe_2O_3 transform to α-Fe_2O_3 at these temperatures, respectively. Figures $6a_1$ and $6b_1$ show the as-prepared gels would yield α-Fe_2O_3 if directly calcined at 500 and 600°C/2 hrs. A pretreatment at 200 or 300°C for 2 hrs eventually resulted in the formation of LFS and Li–γ-Fe_2O_3 that avoided the presence of α-Fe_2O_3 at 500°C (Figs. $6a_2$ and $6a_3$), indicating γ-Fe_2O_3 derived from magnetite

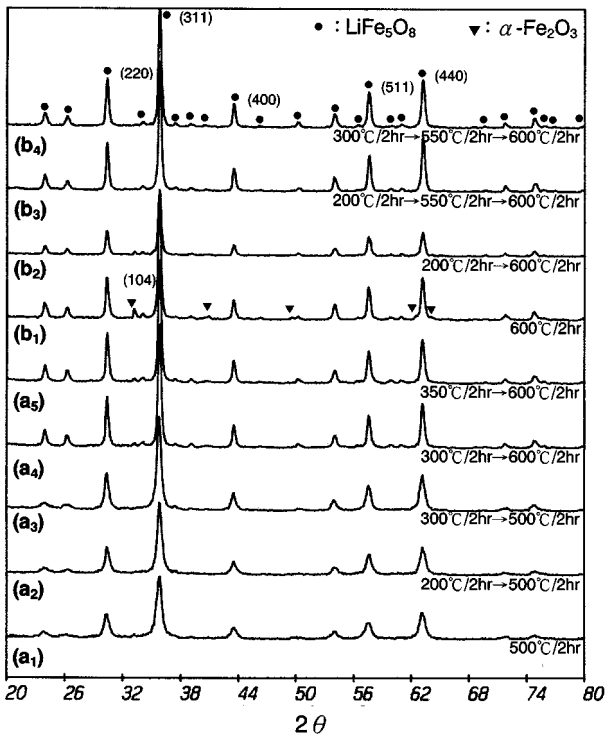

FIG. 6. XRD patterns of the samples demonstrating the possibility of eliminating α-Fe_2O_3 formation using heat pretreatment techniques. Heat-treatment sequences for each sample are indicated under the patterns.

can react with Li^+ to form LFS. Meanwhile, Li–γ-Fe_2O_3 was formed in the same temperature range, because calcination at 600°C/2 hrs for the samples pretreated at 200 and 300°C/2 hrs and even 350°C/2 hrs would yield α-Fe_2O_3 (Figs. $6b_2$ and $6a_4$). Obviously, this resulted from the coexistence of Li–γ-Fe_2O_3. Further heat treatments at 550°C/2 hrs were employed and followed by a check treatment at 600°C/2 hrs. The results proved that monophase lithium ferrite powders could be obtained (Figs. $6b_3$ and $6b_4$). The two-step heat treatment proved that LFS powders can be synthesized at temperatures lower than 600°C using tartrate gel techniques.

At present, both the sequence relationships between the formation of γ-Fe_2O_3 and Li–γ-Fe_2O_3 from its precursor and the formation mechanism for the two iron oxides seem to be vague. However, the DTA/TG curves reveal that γ-Fe_2O_3 appears at a lower temperature as compared to Li–γ-Fe_2O_3. The increase in the amount of γ-Fe_2O_3 formed certainly decreases the amount of Li–γ-Fe_2O_3 formation (Fig. 6). The low-temperature annealing also reveals that LFS and Li–γ-Fe_2O_3 can be obtained at 200 and 300°C/2 hrs, indicating that the formation of γ-Fe_2O_3 and Li–γ-Fe_2O_3 can be initiated at temperatures as low as 200°C (Figs. $7a_2$ and $7a_3$). Once the latter occurs, the temperature required to form LFS must be increased to 550°C. Thus, how to decrease and even eliminate the formation of Li–γ-Fe_2O_3 during the step of low-temperature heat treatment becomes crucial for our study.

An elaboration on eliminating the formation of Li–γ-Fe_2O_3 was undertaken next (37). However, it is interesting to note that the formation of a larger amount of γ-Fe_2O_3 (smaller amount of Li–γ-Fe_2O_3) seems to depend on complete oxidation (weight gain) of the precursor (magnetite) (Fig. 5). Meanwhile, once Li–γ-Fe_2O_3 is formed, the LFS synthesis can be processed only by annealing at temperatures above 550°C (Figs. $6b_3$ and $6b_4$), which is slightly below the temperature for transformation of Li–γ-Fe_2O_3 to form α-Fe_2O_3 (25). The temperature ranges from 200 to 300°C at which γ-Fe_2O_3 forms and LFS forms from γ-Fe_2O_3 (Figs. $6a_2$ and $6a_3$) is also the range for initiating γ- to α-Fe_2O_3 transformation (Figs. 4b and 4c) and covering Li–γ-Fe_2O_3 formation. However, LFS derived from Li–γ-Fe_2O_3 at this temperature range would be very limited. This is because the Li–γ-Fe_2O_3 which appears due to the annealing treatment at the temperature would persist and form α-Fe_2O_3 after calcination at 600°C (Figs. $6b_2$ and $6a_4$). Thus, it is possible to eliminate Li–γ-Fe_2O_3 formation by regulating the oxidation atmosphere. Further, the LFS

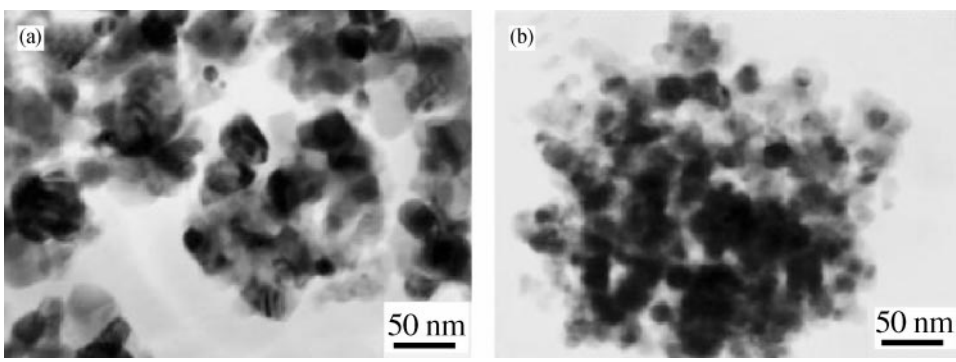

FIG. 7. TEM micrographs of lithium ferrite powders obtained by one-step (a) and two-step (b) processes of heat-treatment at 200 to 300°C and then at 550°C, respectively.

formation uses γ-Fe_2O_3 and Li–γ-Fe_2O_3 as precursors; both proceed individually at temperatures slightly lower than that for the phase transformation. Considering the two possibilities, monophase LFS powders can be obtained by a one-step heat treatment process where the temperature can be lower than 350°C. Figures 7a and 7b demonstrate the transmission electronic micrographs of lithium ferrite powders obtained by one-step and two-step processes of heat treatment at 200 to 300°C and then at 550°C, respectively. Note, the powders may show two different crystallite sizes (ca. 20 nm and ca. 40 nm, Fig. 7a) obtained using one-step processes. The powders may show one crystallite sizes ($\sim$ 20 nm, Fig. 7b) obtained using two-step processes.

3.4. Topotactic Reaction

A spinel-structure to spinel-structure thermal reaction, or topotactic reaction, was anticipated to proceed in LFS synthesis in this study. Superficially, it can be the mechanism that dominates the LFS formation. However, a question which arises is that of why the presence of a certain amount of Li^+ in the γ-Fe_2O_3 structure would substantially increase the formation temperature by 250°C. A rough inference may lead to a conclusion that the presence of Li in γ-Fe_2O_3 may retard the additional Li from entering the γ-Fe_2O_3 structure. However, if the cause for LFS formation from Li–γ-Fe_2O_3 proceeding at such a high temperature is the increase in phase transformation temperature (24), then it can justify the initiation of phase transformation being the dominant factor that triggers the reaction for LFS formation. It is obvious that the topotactic reaction may not be the main route to the LFS formation. It is possible that the Li–γ-Fe_2O_3 decomposes to form γ-Fe_2O_3 again. The γ phase then reacts with Li^+ to form LFS before transforming to α-Fe_2O_3 as it occurs at 200 to 300°C. LFS formation from γ-Fe_2O_3 and Li–γ-Fe_2O_3 can be based on two different processes.

4. CONCLUSIONS

This study examines the characteristics of DTA/TG curves of Li–Fe xerogels during the formation of lithium ferrite powders by tartrate gel techniques. The formation of lithium ferrite was conducted by adjusting the thermal reaction for γ-Fe_2O_3 and Li–γ-Fe_2O_3 with lithium in the temperature range of 200–350°C and $\sim$ 550°C, respectively, by which the formation of α-Fe_2O_3 could be eliminated.

During the thermal reaction, an increase in the amount of γ-Fe_2O_3 formation decreased Li–γ-Fe_2O_3 formation. Whenever the γ phase transformation to α-Fe_2O_3 occurs, higher temperatures of annealing, > 700°C, must be adopted so that the α-Fe_2O_3 can be eliminated.

The thermal reaction for the formation of lithium ferrite can be topotactic. If that is the case, it is more important and necessary that the reaction is triggered by the initiation of the γ- to α-Fe_2O_3 phase transition.

ACKNOWLEDGMENTS

The author thanks Dr. S. I. Hsiang for helpful discussions. This work was sponsored by the National Science Council of the Republic of China under Contract NSC 89-2216-E006-086. Thanks are also extended to C. M. Chen and X. Y. Yao for their assistance in XRD and TEM analyses.

REFERENCES

1. H. J. Masterson, J. G. Lunney, D. Ravinder, and T. M. D. Coey, *J. Magn. Magn. Mater.* **140,** 2081 (1995).
2. G. Balestrino, S. Martellucci, A. Paoletti, P. Paroli, G. Petrocelli, A. Tebano, S. A. Oliver, and C. Vittoria, *Solid State Commun.* **96,** 997 (1995).
3. L. G. Van Uitert, *J. Appl. Phys.* **26,** 1289 (1955).
4. A. D. Schnitzler, V. J. Folen, and G. T. Rado, *J. Appl. Phys.* **33,** 1293 (1962).
5. F. F. Y. Wang, R. L. Gravel, and M. Kestigian, *IEEE Trans. Magn.* **MAG-4,** 55 (1968).
6. R. K. Mishra, O. O. Van der Biest, and G. Thomas, *J. Am. Ceram. Soc.* **61,** 121 (1978).
7. A. J. Pointon and R. C. Saull, *J. Am. Ceram. Soc.* **52,** 157 (1969).
8. A. Goldman, "Modern Ferrite Technology." Van Nostrand Reinhold, New York, 1990.
9. J. J. Ritter and P. Maruthamuthu, *Inorg. Chem.* **34,** 4278 (1995).
10. M. Tabuchi, K. Ado, H. Kobayashi, I. Matsubara, H. Kageyama, M. Wakita, S. Tsutsui, S. Nasu, Y. Takeda, C. Masquelier, A. Hirano, and R. Kanno, *J. Solid State Chem.* **141,** 554 (1998).
11. N. Rezlescu, E. Rezlescu, I. Ciobotaru, M. L. Craus, and P. D. Popa, *Ceram. Int.* **24,** 31 (1998).
12. G. Bonsdorf, H. Langbein, and K. Knese, *Mater. Res. Bull.* **30,** 175 (1995).
13. P. Peshev and M. Pecheva, *Mater. Res. Bull.* **13,** 1167 (1978).
14. H. F. Yu and A. M. Gadalla, *J. Mater. Res.* **11,** 663 (1996).
15. T. Sano and Y. Tamaura, *Mater. Res. Bull.* **34,** 389 (1999).
16. V. Berbenni, A. Marini, G. Bruni, and R. Riccardi, *Thermochim Acta* **346,** 115 (2000).
17. A. Putnis, "Introduction to Mineral Sciences." Cambridge Univ. Press, Cambridge, UK, 1992.
18. A. R. West, "Solid State Chemistry and Its Applications." Wiley, New York, 1986.
19. S. Okamoto, *J. Solid State Chem.* **39,** 240 (1981).
20. K. S. Rane, V. M. S. Verenkar, and P. Y. Sawant, *J. Mater. Sci. Mater. Electron.* **10,** 133 (1999).
21. A. K. Nikumbh, A. D. Aware, and P. L. Sayanekar, *J. Magn. Magn. Mater.* **114,** 27 (1992).
22. T. Tsumura, A. Shimizu, and M. Inagaki, *J. Mater. Chem.* **3,** 995 (1993).
23. J. M. Yang, W. J. Tsuo, and F. S. Yen, *J. Solid State Chem.* **145,** 50 (1999).
24. Y. Yamanobe, K. Yamaguchi, K. Matsumoto, and T. Fujii, *Jpn. J. Appl. Phys. Part* 1 **30,** 478 (1991).
25. P. S. Sidhu, *Clays Clay Miner.* **36,** 31 (1988).
26. Y. Nakatani and M. Matsuoka, *Jpn. J. Appl. Phys.* **22,** 233 (1983).
27. C. Barriga, V. Barron, R. Gancedo, M. Gracia, J. Morales, J. L. Tirado, and J. Torrent, *J. Solid State Chem.* **77,** 132 (1988).

28. W. Zhong, W. Ding, N. Zhang, J. Hong, Q. Yan, and Y. Du, *J. Magn. Magn. Mater.* **168,** 196 (1997).
29. G. Arlt and P. Sasko, *J. Appl. Phys.* **51,** 4956 (1980).
30. S. I. Hsiang and F. S. Yen, *J. Am. Ceram. Soc.* **79,** 1053 (1996).
31. P. Perriat, *Nanostruct. Mater.* **6,** 791 (1995).
32. H. L. Wen and F. S. Yen, *J. Cryst. Growth* **208,** 696 (2000).
33. P. Ayyub, M. S. Multani, M. Barma, V. R. Palkar, and R. Vijayaraghavan, *J. Phys. C*: *Solid State Phys.* **21,** 2229 (1988).
34. M. S. Multani and P. Ayyub, *Condens. Matter News* **1,** 25 (1991).
35. M. Vallet, X. Obradors, M. Pernet, M. Medarde, and J. Rodriguez, *IEEE Trans. Magn.* **24,** 1829 (1988).
36. T. Kodama and Y. Tamura, *J. Am. Ceram. Soc.* **78,** 1335 (1995).
37. F. S. Yen, W. J. Tsuo, and H. J. Kao, "Size Characteristics of Nano-sized Lithium Ferrite Powders Preparaed by Tartrate Gel Techniques," in preparation.